Thermoelectric transport in strongly correlated quantum dot nanocomposites

Jun Zhou and Ronggui Yang*
Department of Mechanical Engineering, University of Colorado, Boulder, Colorado 80309, USA
(Received 25 May 2010; published 25 August 2010)

We investigate the thermoelectric transport properties (electrical conductivity, Seebeck coefficient, power factor, and thermoelectric figure of merit) in strongly correlated quantum dot nanocomposites at low temperature (77 K) by using the dynamical mean-field theory and the Kubo formula. The periodic Anderson model is applied to describe the strongly correlated quantum dot nanocomposites with tunable parameters such as the size of quantum dots and the electron occupation number. The electron occupation number can be controlled by the doping concentration in the both matrix and quantum dots, the size of quantum dots, and the interdot spacing. These parameters control the transition between *n*-type like behavior (with negative Seebeck coefficient) and *p*-type like behavior (with positive Seebeck coefficient) of strongly correlated quantum dot nanocomposites. Large Seebeck coefficient up to 260 μV/K due to the asymmetry of the electron bands with sharp electron density of states can be obtained in the strongly correlated quantum dot nanocomposites, along with moderate electrical conductivity values in the order of $10^5/\Omega$ m. This results in optimal power factor about 78 μW/cm K^2 and optimal figure of merit (*ZT*) over 0.55 which is much larger than the value of the state-of-the-art low-temperature thermoelectric materials. This study shows that high efficiency thermoelectric materials at low temperature can be obtained in strongly correlated quantum dot nanocomposites.

DOI: 10.1103/PhysRevB.82.075324 PACS number(s): 72.15.Jf, 71.10.Fd, 72.10.−d

I. INTRODUCTION

Potentially enhanced thermoelectric (TE) properties in strongly correlated electron systems has been proposed and studied both experimentally and theoretically.[1–4] When the Coulomb interaction *U* between charge carriers is larger than their kinetic energy E_k, the system is considered to be strongly correlated electron systems.[5] Generally, there are two kinds of strongly correlated electron systems: Kondo impurity system and Kondo lattice system. The Kondo impurity system in which dilute localized magnetic impurities are dispersed in nonmagnetic metal has been investigated since 1960s.[6] The Kondo effect due to the spin-flip scattering between the conduction electrons in metal and the localized electrons in impurities is observed which results in a large Seebeck coefficient and a minima in electrical resistivity.[4,7,8] Different from Kondo impurity system, the magnetic moments in Kondo lattice system are well located on lattice sites rather than randomly and dilutely distributed. The intersite correlation and the coherent effect due to the periodicity of localized electrons in Kondo lattice system result in very different quantum behaviors from Kondo impurity system at low temperature.[4] The Hubbard model[5] and the Anderson model[9] are commonly used to describe the electron performance in strongly correlated electron system. Large Seebeck coefficient due to the Kondo effect has also been found in Kondo lattice system at low temperature.[2,10,11] Earlier studies of localized magnetic moments in both Kondo impurity system and Kondo lattice system have been focused on *d*- or *f*-orbital electrons in transition metals or rare-earth elements. Recently, Kondo effect in quantum dots (QDs) has been studied extensively.[12–17] In this paper, we are interested in exploring the Kondo effect in strongly correlated quantum dot nanocomposites for thermoelectricity, especially for low-temperature applications which appears to be a significant challenge in high-efficiency TE material development.

Many efforts have been devoted to improve the TE energy conversion efficiency in low-dimensional materials systems including nanowires,[18,19] superlattices,[20] and QD superlattices.[21,22] For example, Harman *et al.*[21,22] found remarkable enhancements of TE figure of merit (*ZT*) in PbSeTe-based QD superlattices prepared by molecular beam epitaxy. Yet another endeavor in low-dimensional TE research is to model and synthesize high-efficiency TE nanocomposites, which could potentially be more cost effectively produced. Theoretical models have been proposed to study phonon thermal conductivity[23–25] and electron power factors,[26–31] on these low-dimensional materials, mostly based on Boltzmann transport theory. Significant experimental progress has been made and most work attributed the *ZT* enhancement to the reduction of lattice thermal conductivity while some work also showed the increase in Seebeck coefficient.[32–35] It is believed that the sharp density of states (DOS) close to the chemical potential in the low-dimensional systems (QDs, nanowires, and superlattices) is the major contributor for electronic power factor enhancement.[32] Possible enhancement of Seebeck coefficient due to the formation of electronic minibands that can achieve better configuration of DOS for TE (Ref. 36) in three dimensionally regimented QDs with strong interdot couplings has been studied by Balandin *et al.*[37] and Yadav *et al.*[38] They solved the Schrödinger equation under the envelope function effective-mass approximation for electron spectrum and then calculated the TE transport properties semiclassically by solving the Boltzmann equation. Similarly, Gómez[39] used the transfer matrix formalism to study the electron miniband formation.

In this paper, we study the TE transport properties in strongly correlated quantum dot nanocomposites at liquid nitrogen temperature (77 K), which could potentially address the challenges in low-temperature TE materials development. Generally speaking, quantum dot nanocomposites system is a special nanocomposites material whose inclusions

TABLE I. Transport regimes in quantum dot nanocomposites with different interdot coupling strength, and intradot Coulomb interaction (correlation strength). Here, a is the distance between QDs, D is the diameter of QDs, l_ψ is the length of the extended wave function of localized electron in the matrix material, l_{ind} is the indirect coupling length between QDs intermediated by the matrix material, U is the Coulomb interaction, and E_k is the kinetic energy of electrons.

Regime	Interdot coupling	Intradot interaction
[a] Hopping (Ref. 40)	$a-D>l_{ind}>l_\psi$	$U \ll E_k$
[b] Miniband formation (Ref. 37)	$a-D<l_\psi<l_{ind}$	$U \ll E_k$
[c] Hubbard model (Ref. 41)	$a-D<l_\psi<l_{ind}$	$U>E_k$
[d] Anderson model (Ref. 10)	$l_\psi<a-D<l_{ind}$	$U>E_k$

are well "*quantum confined*" in comparison with conventional nanocomposites materials whose inclusions can be treated as normal impurities without quantum effects. According to different conditions such as the interdot coupling strength and intradot Coulomb interaction strength, the electron-transport regimes in quantum dot nanocomposites can be divided into several categories as shown in Table I when the QDs are uniform in size, and densely and orderly regimented in a matrix material. The interdot coupling highly depends on both the matrix and the dot materials. For example, it could be weak for PbSe QDs with hydrazine as matrix material[40] and could be very strong for PbSeTe QDs with PbTe as matrix material.[21] It also depends on the interdot spacing. There are two mechanisms in interdot coupling: direct coupling and indirect coupling. The direct interdot coupling is mainly due to the overlap of the extended electron wave functions of the neighboring QDs. The coupling strength could be roughly proportional to $\exp[-(a-D)/l_\psi]$, where a is the interdot distance, D is the diameter of QD, and l_ψ is the decay length of the extended wave function. The indirect interdot coupling originates from the matrix material intermediated correlation between QDs such as Ruderman-Kittel-Kasuya-Yosida interaction[42] whose coupling strength approximately decays as $(a-D)^{-3}$. We approximate the decay length of this correlation as $l_{ind} \sim 1/k_F$ where k_F is the Fermi wave vector. Usually, l_{ind} is several times larger than l_ψ. When $a-D>l_{ind}>l_\psi$ and $U \ll E_k$ (case [a] in Table I), both the interdot coupling and the intradot Coulomb interaction are weak. We will expect low electrical conductivity (in the order of $1/\Omega$ m which is in the insulator regime) although Seebeck coefficient could be as high as the order of 1000 μV/K (Ref. 40) due to the hopping mechanism.[43] If $a-D<l_\psi<l_{ind}$ and $U \ll E_k$ (case [b] in Table I), the interdot coupling is strong but the intradot Coulomb interaction is weak. The localized discrete states in individual QDs will form extended electron states that results in the formation of minibands[37] whose bandwidth is in the same order of the coupling strength. The formation of extended states and minibands in QD arrays has been observed experimentally[43] and the well-separated minibands of relatively large band width are believed to be favorable for the TE efficiency improvement[37] comparing to its bulk counterpart because of a sharp DOS located near the chemical potential. If $a-D<l_\psi<l_{ind}$ and $U>E_k$ (case [c] in Table I), the direct interdot coupling plays a dominant role and the intradot Coulomb interaction is strong. The Hubbard model[5,41] can be used to describe such a system when the contribution on electron transport by the matrix material is negligible. When $l_\psi<a-D<l_{ind}$ (case [d] in Table I), the electrons in the QDs could still couple with each other but indirectly through the intermediate matrix materials. In this case, the periodic Anderson model which is the extension of the Anderson model to a lattice can be a promising candidate to describe the electron behavior in the strongly correlated quantum dot nanocomposites material.[4]

It is interesting to note that the periodic Anderson model has been used to study transition metals and a very large Seebeck coefficient (about 500 μV/K) has been obtained.[10] Cai and Mahan[44,45] recently proposed one kind of Anderson model, which is different from periodic Anderson model, to study electronic properties of QD arrays. They assumed a complex lattice with two lattice sites which is different from the simple lattice in periodic Anderson model. In their model, the QDs are treated as correlated sites and the conduction electrons in matrix are treated as link sites. With the energy levels and the Coulomb interactions as input parameters, they found that the QD array material can be metallic with a large Seebeck coefficient. Here we used the periodic Anderson model to study TE transport in the strongly correlated quantum dot nanocomposites. Different from references,[44,45] the QD and the conduction electrons in the same unit are treated as the same site in periodic Anderson model. We expect that a large Seebeck coefficient in the strongly correlated quantum dot nanocomposites since it essentially takes advantage of the energy-sensitive scattering due to the Kondo effect (such as case [c]) and the sharp DOS in electronic band structures (such as cases [a] and [b]).

This paper is organized as follows. In Sec. II, we present a periodic Anderson model-based model to study the electronic band structures in quantum dot nanocomposites system that is numerically solved by the dynamic mean-field theory. Then the equations for TE transport properties are presented based on the standard Kubo formula. In Sec. III, we first discuss the band structure, the electron occupation number, and the energy dependence of the Kondo scattering. Then we study the transport properties such as electrical conductivity, Seebeck coefficient, power factor, and TE figure of merit ZT as functions of the size of QDs and electron occupation number in detail. Finally, Section IV concludes this paper.

II. MODEL

Figure 1(a) shows a strongly correlated quantum dot nanocomposites with the uniformly sized QDs embedded in a quantum dot nanocomposites as periodic Anderson impurities in a three-dimensional cubic lattice. The distance between the nearest-neighboring QDs is a. In other words, each QD is located at the center of a cubic unit cell with size a. Figure 1(b) shows the band diagram of the quantum dot nanocomposites, large energy barriers confines the energy

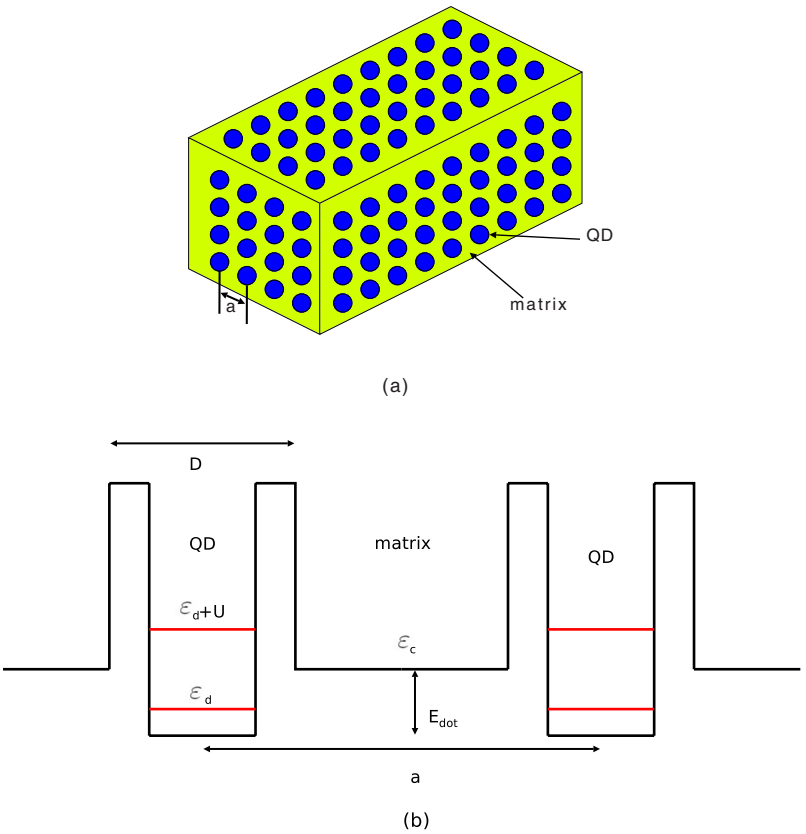

FIG. 1. (Color online) (a) Schematic of simple cubic lattice quantum dot nanocomposites with QDs periodically distributed in the matrix. The dots represent spherical QDs with a size D. The distance between the nearest-neighboring QDs is a. (b) Schematic band diagram of the quantum dot nanocomposites with the lowest two energy levels in QDs. ε_d is the energy level of the localized electron in QD, U is the Coulomb interaction, ε_c is the conduction band minima in matrix, E_{dot} is the energy difference between the conduction band minima of QD material and ε_c, and D is the diameter of the QD.

levels in QDs. ε_c denotes the of conduction-band minima of the matrix material and E_{dot} is the energy difference between the conduction-band minima of QD material and the matrix material. ε_d denotes the single-particle energy level of localized electron in QD and U denotes the on-site Coulomb repulsion between electrons with different spin orientations in the same QD. We study the TE transport properties of strongly correlated quantum dot nanocomposites using different set of parameters, ε_c, ε_d, and U, which are the dominant parameters in periodic Anderson model. These parameters can be controlled by the size of QDs (Ref. 46) approximately as shown below

$$\varepsilon_c = 0, \tag{1a}$$

$$\varepsilon_d = -E_{dot} + \frac{\hbar^2 \pi^2}{2mD^2}, \tag{1b}$$

$$U = \frac{e^2}{4\pi\epsilon D/2}. \tag{1c}$$

Here m is the effective mass of electron, ϵ is the dielectric constant in QD, e is the carrier charge of electron, and $\hbar$ is the Planck constant.

The standard periodic Anderson model Hamiltonian consisting of the kinetic terms of both conduction electrons in the matrix and localized electrons in QDs, the correlation term, and the hybridization term can be written as

$$H = \sum_{\vec{k}s} \varepsilon_{\vec{k}s} c^{\dagger}_{\vec{k}s} c_{\vec{k}s} + \sum_{is} \varepsilon_d d^{\dagger}_{is} d_{is} + \frac{U}{2} \sum_{is} n^d_{is} n^d_{i-s} + V \sum_{is} (d^{\dagger}_{is} c_{is} + c^{\dagger}_{is} d_{is}). \tag{2}$$

Here, $c^{\dagger}_{\vec{k}s}(c_{\vec{k}s})$ creates (annihilates) a conduction electron in matrix with spin $s = \pm 1$ which means spin up and spin down, momentum $\vec{k}$ in momentum space, and kinetic energy $\varepsilon_{\vec{k}s}$ which is centered at ε_c. $c^{\dagger}_{is}(c_{is})$ creates (annihilates) a conduction electron and $d^{\dagger}_{is}(d_{is})$ creates (annihilates) a localized electron in the QD with spin s at site i in real space, n^d_{is} is the localized electron occupation operator. The hybridization term describes the coupling between the conduction electrons in matrix and the localized electrons in QDs. The matrix element of hybridization is generalized to V while the strong correlation term is induced by the Coulomb interaction U. In a three-dimensional simple cubic lattice with nearest-neighbor hopping, the hybridization term scales as $V = \frac{t}{\sqrt{6}}$,[47] where t is hybridization constant. In this paper, we consider t as input parameter. Usually, its value is from tens of millielectron volt to hundreds of millielectron volt.[48] It should be emphasized that a constant t is valid only when $\varepsilon_d \leq \mu \leq \varepsilon_d + U$, where μ is the chemical potential.

It is well known that there is no exact analytical solutions for the periodic Anderson model with finite U.[47] Here we use the dynamical mean-field theory which is widely used in the study of variety of strongly correlated lattice fermion models[47] to solve the periodic Anderson model numerically.[49] The Green's functions and spectral functions

at finite temperature are calculated by the open source code from Ref. 47. Under the local approximation in dynamical mean-field theory,[50,51] the k-dependent self-energy of localized electron $\Sigma_s^d(\vec{k},z)$ is approximated by k-independent one $\Sigma_s^d(z)$. Such approximation is justified when a three-dimensional lattice is considered ($d=3$) according to the results in Refs. 50 and 51. Then the exact Green's function of the conduction electrons $G_s^c(\varepsilon_{\vec{k}},z)$ and localized electrons $G_s^d(\varepsilon_{\vec{k}},z)$ for the periodic Anderson model Hamiltonian Eq. (2) can then be written as[52]

$$G_s^c(\varepsilon_{\vec{k}},z)=\frac{1}{z-\varepsilon_{\vec{k}s}-\sum_s^c(z)}, \tag{3a}$$

$$G_s^d(\varepsilon_{\vec{k}},z)=\frac{1}{z-\varepsilon_d-\sum_s^d(z)-|V|^2/(z-\varepsilon_{\vec{k}s})}, \tag{3b}$$

where z is the Matsubara frequency which is a complex number slightly off the real axis. The self-energy of conduction electrons in Eq. (3a) is

$$\sum_s^c(z)=\frac{|V|^2}{z-\varepsilon_d-\sum_s^d(z)}. \tag{4}$$

From Eqs. (3a) and (3b) and the self-energy $\Sigma_s^c(z)$, the local Green's function can be written as

$$G_s^c(z)=\frac{1}{N}\sum_{\vec{k}}G_s^c(\varepsilon_{\vec{k}},z)=\int_{-\infty}^{\infty}d\varepsilon_k\frac{P(\varepsilon_k)}{z-\varepsilon_k-\sum_s^c(z)}, \tag{5a}$$

$$G_s^d(z)=\frac{1}{N}\sum_{\vec{k}}G_s^d(\varepsilon_{\vec{k}},z)=\int_{-\infty}^{\infty}d\varepsilon_k\frac{P(\varepsilon_k)}{z-\varepsilon_d-\sum_s^d(z)-|V|^2/(z-\varepsilon_k)}. \tag{5b}$$

Here, $P(\varepsilon_k)$ is the Gaussian-type noninteracting tight-binding DOS (Refs. 47 and 53),

$$P(\varepsilon_k)=\frac{1}{\sqrt{2\pi}t}\exp\left(-\frac{\varepsilon_k}{2t^2}\right). \tag{6}$$

In dynamical mean-field theory, the local Green's function of the localized electrons must be equal to the corresponding Green's function of effective single-impurity Anderson model[47] due to the self-consistency condition. The latter one can be defined as

$$G_s^d(z)=G_{\mathrm{SIAM}}(z)=\frac{1}{z-\varepsilon_d-\Delta_s(z)-\sum_s^d(z)}, \tag{7}$$

where $\Delta(z)$ is the hybridization function.

The self-energy $\Sigma_s^d(z)$ is determined by self-consistent iterations. For an initial $\Sigma_s^d(z)$, one can calculate $G_s^d(z)$ by using Eq. (5b), then $\Delta(z)$ can be obtained through Eq. (7). By using the updated $\Delta(z)$ as a new input in solving the effective single-impurity Anderson model, a new $\Sigma_s^d(z)$ can be obtained. By repeating these steps until the self-consistency condition is fulfilled, a converged $\Sigma_s^d(z)$ is obtained.

In order to include other scattering mechanisms such as the electron-impurity scattering and the electron-phonon scattering, we introduce an extra finite image part $i\delta$ in self-energy[2,45]

$$\sum_s^d(z)\to\sum_s^d(z)-i\delta. \tag{8}$$

δ can be interpreted as the inverse scattering time of the scatterings besides the Kondo scattering.

After obtaining the converged $\Sigma_s^d(z)$, the Green's functions in Eqs. (5a) and (5b) could be obtained. One can then determine the chemical potential and calculate the TE transport properties. The k-independent spectral functions for the conduction and localized electrons are coming from the imaginary parts of the local Green's functions,

$$A_s^c(\omega)=-\frac{1}{\pi}\mathrm{Im}\,G_s^c(\omega+i0^+), \tag{9a}$$

$$A_s^d(\omega)=-\frac{1}{\pi}\mathrm{Im}\,G_s^d(\omega+i0^+). \tag{9b}$$

For a fixed local total electron occupation number $n_{tot}=n^c+n^d=\Sigma_s(n_s^c+n_s^d)$, the chemical potential μ can be self-consistently determined by

$$n_s^c=\langle c_{is}^\dagger c_{is}\rangle=\int_{-\infty}^{\infty}d\omega f(\omega)A_s^c(\omega), \tag{10a}$$

$$n_s^d=\langle d_{is}^\dagger d_{is}\rangle=\int_{-\infty}^{\infty}d\omega f(\omega)A_s^d(\omega), \tag{10b}$$

where $f(\omega)=[\exp(\omega-\mu)/k_bT+1]^{-1}$ is Fermi-Dirac distribution, k_b is Boltzmann constant, and T is the absolute temperature.

The TE transport properties at finite temperatures can then be calculated using the linear-response theory—the Kubo formula.[54] The definition of the electrical current $\vec{j}$ and the heat current $\vec{j}_q$ can be written as[55]

$$\vec{j}=\frac{e}{\hbar}\sum_{\vec{k},s}\nabla_{\vec{k}}\varepsilon_{\vec{k}}c_{\vec{k}s}^\dagger c_{\vec{k}s}, \tag{11a}$$

$$\vec{j}_q=\frac{1}{\hbar}\sum_{\vec{k},s}(\varepsilon_{\vec{k}}-\mu)\nabla_{\vec{k}}\varepsilon_{\vec{k}}c_{\vec{k}s}^\dagger c_{\vec{k}s}. \tag{11b}$$

In our calculation, we ignore the k-independent hybridization term that means the localized electrons do not contribute to the current directly.[2] According to the linear-response theory, the electrical current density $\vec{J}$ and the heat current density $\vec{J}_q$ depend linearly on the electric field $\vec{E}$ and the temperature gradient ∇T,

$$\vec{J}=L^{11}\vec{E}+L^{12}(-1/T\nabla T), \tag{12a}$$

$$\vec{J}_q=L^{21}\vec{E}+L^{22}(-1/T\nabla T). \tag{12b}$$

We have $L^{12}=L^{21}$ according to Onsager relation. L^{11}, L^{12}, and L^{22} can be expressed as[2]

$$L^{11} = \frac{e^2}{\hbar a}\int_{-\infty}^{\infty}[-f'(\omega)]\Xi(\omega)d\omega, \tag{13a}$$

$$L^{12} = \frac{e}{\hbar a}\int_{-\infty}^{\infty}[-f'(\omega)](\omega-\mu)\Xi(\omega)d\omega, \tag{13b}$$

$$L^{22} = \frac{1}{\hbar a}\int_{-\infty}^{\infty}[-f'(\omega)](\omega-\mu)^2\Xi(\omega)d\omega. \tag{13c}$$

Then the isotropic electrical conductivity, the Seebeck coefficient, and the electronic thermal conductivity can be easily obtained as $\sigma=L^{11}$, $S=L^{12}/TL^{11}$, and $\kappa_e=[L^{22}-(L^{12})^2/L^{11}]/T$. The transport distribution function (TDF) $\Xi(\omega)$ in Eqs. (13a)–(13c) can be obtained by

$$\Xi(\omega) = \frac{2\pi}{d}t^2\int_{-\infty}^{\infty}\rho(\varepsilon_k)A_c^2(\varepsilon_k,\omega)d\varepsilon, \tag{14}$$

where the k-dependent spectral function for the conduction electrons in Eq. (14) is from the imaginary part of Green's function in Eq. (3a),

$$A_c(\varepsilon_{\vec{k}},\omega) = -\frac{1}{\pi}\mathrm{Im}\, G_s^c(\varepsilon_{\vec{k}},\omega+i0^+). \tag{15}$$

It should be emphasized that the Kondo effect is very sensitive to temperature,[56] it becomes weaker as temperature increases until vanishes when the temperature is above the Kondo temperature T_k. In periodic Anderson model, the Kondo temperature can be roughly estimated in the order of $0.1U$.[45,57] Obviously, smaller size of QDs and smaller ϵ are preferred in order to get larger U and thus higher T_k according to Eq. (1c). In this paper, U is always above 0.07 eV when $D<5$ nm that we considered, $k_bT=6.6$ meV when $T=77$ K. In other words, $k_bT<0.1U$ is always satisfied in our calculation.

III. RESULTS AND DISCUSSIONS

In our sample calculation, we study the TE properties of CdS/CdSe quantum dot nanocomposites with CdS QDs periodically distributed in CdSe matrix material. CdS has an effective mass of electrons $m=0.195m_e$ and a small dielectric constant $\epsilon=8.48\epsilon_0$ at 77 K where m_e is the free-electron mass and ϵ_0 is the vacuum permittivity.[58] E_{dot} is chosen to be 0.163 eV. Under our chosen material properties, $\varepsilon_d-\varepsilon_c=-U/2$ can be satisfied when $D=4$ nm, and $k_bT<0.1U$ can be satisfied when $D<5$ nm. CdS/CdSe could be a good material system worthy of study for the TE transport in strongly correlated quantum dot nanocomposites at low temperature since they have small dielectric constants and CdS QDs can be made relatively easily.[59] Although CdS or CdSe themselves are not a good bulk TE materials, we expect high-efficiency ZT from CdS/CdSe strongly correlated quantum dot nanocomposites since nanostructuring of materials have shown great promises in turning nonthermoelectric materials into high efficiency TE materials, such as silicon and III-V nanomaterials.[18,19] We choose $\delta=3.6$ meV which corresponding to the relaxation time about 0.183 ps ($\sim\hbar/\delta$) which is directly calculated from the experimental mobility of 1650 $\mathrm{cm^2\ V^{-1}\ S^{-1}}$ at 77 K (Ref. 60) to account for the other scattering mechanisms discussed earlier. The hybridization constant is chosen for $t=0.05$ eV throughout the paper unless specified, which is in the same order of the hopping matrix elements between localized states in extended systems from first-principles calculation.[48]

A. Band structure, chemical potential, and Kondo scattering

The Seebeck coefficient of a material is a measure of the asymmetry of the electronic band structure.[1] In order to study the formation of the asymmetric conduction band that is in favor for good TE properties, we show the typical DOS of conduction electrons in Fig. 2 for different cases. The DOS of conduction electrons can be obtained as $[A_\uparrow^c(\omega)+A_\downarrow^c(\omega)]/a^3$, where $A_\uparrow^c(\omega)$ and $A_\downarrow^c$ are determined in Eq. (9a). Figure 2(a) exhibits particle-hole symmetry for different t when $n_{tot}=2$ and $D=4$ nm, as $\varepsilon_d-\varepsilon_c=-U/2$ is satisfied. The chemical potentials for all the three cases are at 0 eV around which there is a narrow gap due to the Kondo resonance.[47] Figure 2(a) also shows that the width of the band is proportional to the hybridization constant t and the height is inversely proportional to it. The smaller the hybridization constant t is, the sharper is the DOS. Figure 2(b) shows the particle-hole asymmetry when $D=3.6$ nm. According to Eqs. (10a) and (10b), the chemical potentials can be calculated to be around 0.099 eV, 0.099 eV, and 0.108 eV, for $t=0.03$ eV, 0.04 eV and 0.05 eV cases, respectively. Clearly, the symmetry of DOS is broken. The DOS for electron energy lower than μ becomes wider and the DOS for higher-energy electrons becomes very narrow and sharp in comparison with the symmetric case. This asymmetry comes from the inequality of $\varepsilon_d-\varepsilon_c>-U/2$ as both ε_d and U increase when D becomes smaller than 4 nm according to Eqs. (1b) and (1c). Figure 2(c) shows the DOS for different D when $n_{tot}=2$. The chemical potentials for $D=3.6$ nm, 4 nm and 4.4 nm cases are calculated to be around 0.058 eV, 0 eV and −0.047 eV, respectively. For small D, μ is positive since $\varepsilon_d-\varepsilon_c>-U/2$ that leads to more electrons distributing in the matrix material, and for large D, μ is negative since $\varepsilon_d-\varepsilon_c<-U/2$ that leads to less electrons distributing in the matrix material. All the cases in Figs. 2(a)–2(c) are half filled, i.e., with $n_{tot}=2$. The symmetry of DOS can also be destroyed by varying n_{tot}. In order to study the general filling, the DOS for different n_{tot} with a fixed $D=4$ nm are also shown in Fig. 2(d). The chemical potentials for $n_{tot}=1.6$, 1.8, and 2 cases are around −0.0258 eV, −0.0123 eV, and 0 eV, respectively. All the above demonstrated that the particle-hole asymmetry of the electron band in the strongly correlated quantum dot nanocomposites can be tuned by both the size of the QDs D and the electron occupation number n_{tot}, which could be used to tune the TE performance as the Seebeck coefficient is a measure of the electron band DOS asymmetry.[1]

After the band structure is calculated, we now study the chemical potential as a function of D and n_{tot} as shown in Fig. 3. Figure 3(a) shows that μ always decreases with D. When D increases, ε_d shifts to lower energy, more electrons

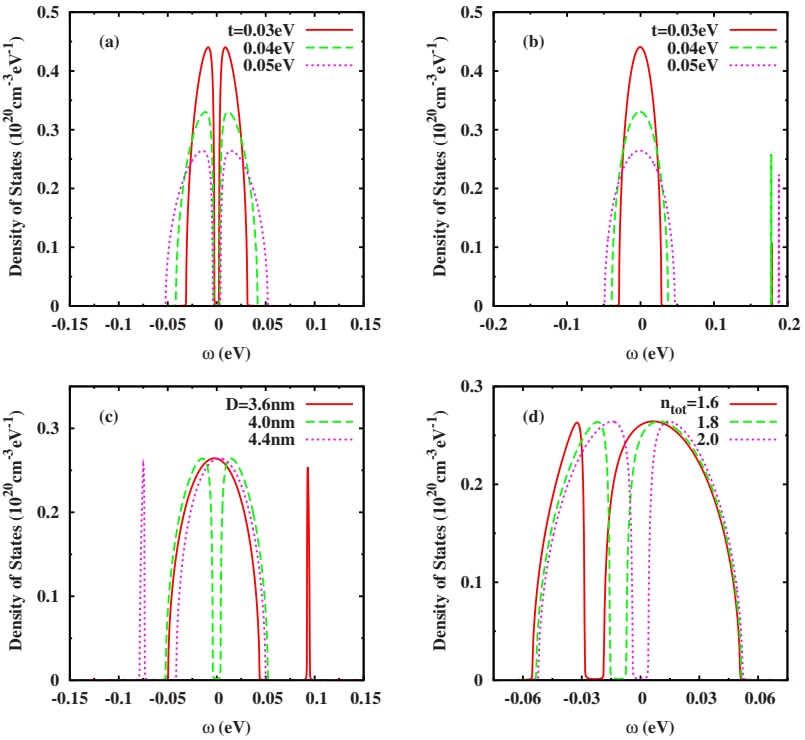

FIG. 2. (Color online) DOS of conduction electrons for different hybridization constant t when $n_{tot}=2$ and (a) $D=4$ nm, (b) $D=3.6$ nm. (c) DOS of conduction electrons for different D when $n_{tot}=2$ and $t=0.05$ eV. (d) DOS of conduction electrons for different n_{tot} when $D=4$ nm and $t=0.05$ eV. All cases used $T=77$ K and $a=10$ nm for calculations.

distribute in QDs and less electrons distribute in matrix, which results in shifting μ to a lower energy. Figure 3(b) shows that μ always increases with the increase in n_{tot} for all D because more electrons distribute in matrix when n_{tot} becomes larger. In the appendix, we present the electron distribution (macroscopically electron concentration) in both the QDs and the matrix material as functions of D, n_{tot}, and a.

We discuss next the energy dependence of the Kondo scattering in the strongly correlated quantum dot nanocomposites. Figure 4(a) shows the DOS in QD for different D. For the particle-hole symmetric case ($n_{tot}=2$ and $D=4$ nm), there are two symmetric peaks and one gap near $\mu=0$. For the asymmetric case of $D=3.6$ nm when μ is located around 0.058 eV, the low-energy peak of DOS almost disappears while the high-energy peak becomes large and sharp. For the asymmetric case of $D=4.4$ nm when μ is around −0.047 eV, the high-energy peak of DOS disappears while the low-energy peak becomes large and sharp. This is because the real part of self-energy $\mathrm{Re}\Sigma_s^d(z)$ shifts the peak of DOS and the image part $\mathrm{Im}\Sigma_s^d(z)$ modifies the amplitude of DOS in Eq. (3b). Usually, the scattering rate (the inverse of the carrier lifetime) of the conduction electrons due to localized electrons is proportional to the DOS of localized electrons.[54] Such scattering can be characterized by TDF Ξ shown in Fig. 4(b). For symmetric case, there are two weak symmetric peaks of Ξ located at ± 0.03 eV while $\mu=0$ is exactly at the center between these two peaks. A zero Seebeck coefficient is expected since the contributions from electrons above the chemical potential and those below the chemical potential cancel with each other as expected from Eq. (13b). Ξ for $D=3.6$ nm displays a large peak at −0.02 eV and a small peak at positive energy since the large DOS of localized electrons at positive energy that suppress Ξ. From Eq. (13b), one could expect that a positive Seebeck coefficient can be obtained as the peak of Ξ is 0.078 eV below μ. Similarly, a negative Seebeck coefficient could be expected as the peak of Ξ is 0.069 eV above μ for $D=4.4$ nm. Interestingly, we could find the p-type like behavior in quantum dot nanocomposites with small D while n-type like behavior with large D when n_{tot} is fixed. Figures 4(c) and 4(d) show the DOS in QDs and the corresponding Ξ for different n_{tot} when $D=4$ nm. Figure 4(c) shows that,

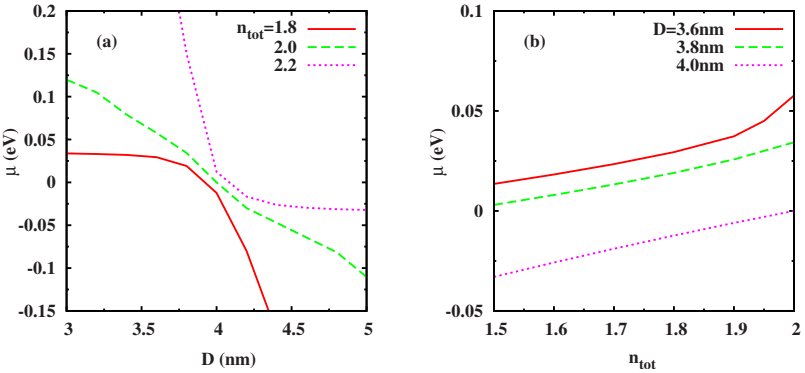

FIG. 3. (Color online) The dependence of chemical potential on (a) the size of QDs D for different electron occupation number $n_{tot}=1.8$, 2, and 2.2, and (b) n_{tot} for different size of QDs $D=3.6$, 3.8, and 4 nm. The calculation uses $t=0.05$ eV, $T=77$ K, and $a=10$ nm.

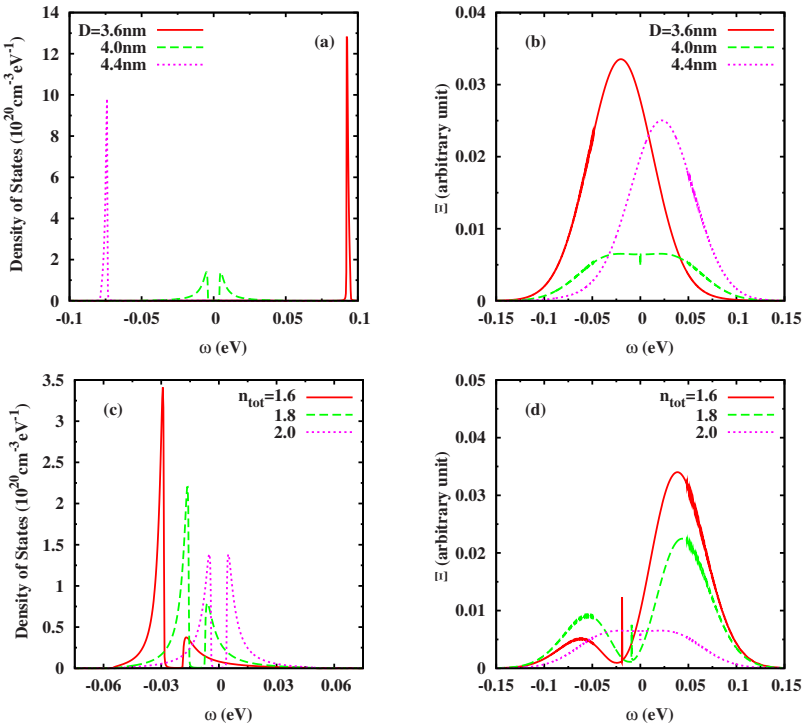

FIG. 4. (Color online) (a) DOS in QD as a function of the size of QDs D when $n_{tot}=2$, (b) TDF as a function of the size of QDs D when $n_{tot}=2$, (c) DOS in QD for different n_{tot} when $D=4$ nm, (d) TDF for different n_{tot} when $D=4$ nm. All the calculations used $a=10$ nm, $t=0.05$ eV, and $T=77$ K.

when n_{tot} decreases, the DOS of localized electrons shifts to lower energy and becomes sharper. Therefore, Ξ for electrons below μ can be suppressed and Ξ for electrons above μ can be maintained for smaller n_{tot} as shown in Fig. 4(d). For example, the location of main peak of Ξ is 0.044 eV which is 0.0563 eV above $\mu=-0.0123$ eV for $n_{tot}=1.8$. Apparently n-type like behavior could be expected with small n_{tot} and p-type like behavior could be expected with large n_{tot} in quantum dot nanocomposites when D is fixed. Moreover, one can also see that the peak of Ξ becomes higher and wider as shown in Figs. 4(b) and 4(d) when the deviation from particle hole symmetric case becomes larger. This feature affects the TE transport properties that we will discuss in next section.

The above results demonstrated that the asymmetry of band structure, the chemical potential, and the energy dependence of the Kondo scattering [characterized by the sharp peak of $\Xi(\omega)$] can be tuned by varying the size of QDs D and the electron occupation number n_{tot}. As a result, the TE transport properties which are directly related to μ and $\Xi(\omega)$ [see Eqs. (13a) and (13b)] can apparently be tuned by D and n_{tot}, which will be shown in the next section.

B. Transport properties

From Eqs. (13a) and (13b), one can find that the direct relation between the transport properties (electrical conductivity and Seebeck coefficient) and the interdot spacing a is quite simple: $\sigma \sim 1/a$ and S does not depend on a. However, σ and S can vary with a indirectly through n_{tot}, as discussed in the Appendix. Therefore, we do not study the a dependence of transport properties in this section, and just choose $a=10$ nm in the following calculation. Figure 5 shows the dependence of electrical conductivity and Seebeck coefficient on the size of QDs D when $n_{tot}=1.8$, 2, and 2.2. The results of that $D<4$ nm for $n_{tot}=1.8$, $D>4.8$ nm for $n_{tot}=2$, and $D>4$ nm for $n_{tot}=2.2$ are not presented in the figures since $\varepsilon_d \leq \mu \leq \varepsilon_d + U$ is not satisfied that makes the constant hybridization approximation invalid. Equations (13a) and (13b) clearly indicates that σ and S are determined by the TDF Ξ and the chemical potential μ. When the peak of Ξ is close to μ (within $3k_bT$), the variation in the amplitude of Ξ and its distance to μ dominate the transport properties. When the peak of Ξ is far away from μ (over $3k_bT$), σ is expected to be very small although S could be large. For $n_{tot}=2$ case, σ reaches a minimum about $0.65\times10^5/\Omega$ m

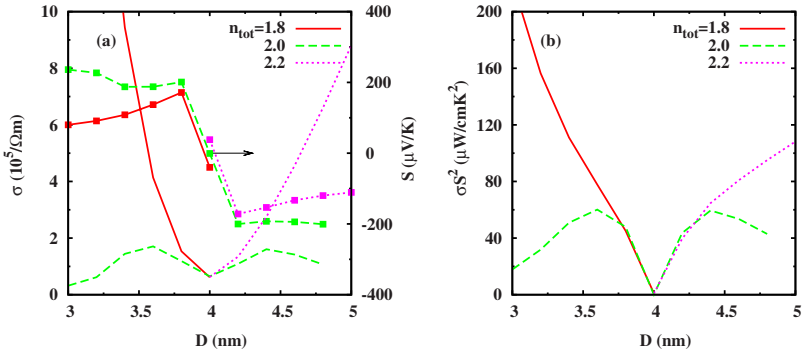

FIG. 5. (Color online) The dependence of (a) electrical conductivity and Seebeck coefficient, and (b) power factor on the size of the QDs D for different electron occupation number $n_{tot}=1.8$, 2, and 2.2. The calculation uses inputs as $a=10$ nm, $\delta=3.6$ meV, $t=0.05$ eV, and $T=77$ K.

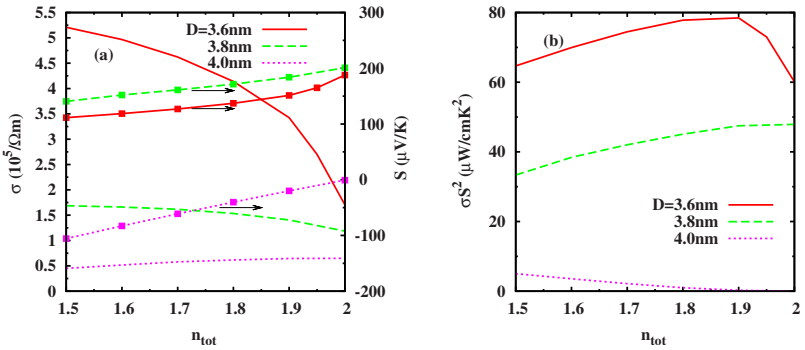

FIG. 6. (Color online) The dependence of (a) electrical conductivity and Seebeck coefficient, and (b) power factor on n_{tot} for different size of QDs $D=3.6$, 3.8, and 4 nm. The calculation uses inputs as $a=10$ nm, $\delta=3.6$ meV, $t=0.05$ eV, and $T=77$ K.

near $D=4$ nm because the amplitude of Ξ for symmetric case is smaller than the asymmetric case as shown in Fig. 4(b) when $3.6<D<4.4$ nm. For $D<3.6$ nm, σ decreases when D decreases, and for $D>4.4$ nm, σ decreases when D increases, due to the fact that the distance between μ and Ξ becomes larger. A maximum σ can thus be obtained near $D=3.6$ nm and $D=4.4$ nm. The maximum of σ is expected to take place when D is smaller than 3 nm for $n_{tot}=1.8$ and when D is larger than 5 nm for $n_{tot}=2.2$ that are not shown in the figure. Figure 5(a) shows that the Seebeck coefficient S decreases with D from a positive value (p-type like) to a negative one (n-type like) when $3.8<D<4.2$ nm. The absolute Seebeck coefficient could be as large as 260 μV/K, as a result of the increase in distance between the peak Ξ and μ. When $D>4.2$ nm or $D<3.8$ nm, the increase in the amplitude of Ξ will cancel the above effect that leads a slightly change in S. Figure 5(b) shows the dependence of the power factor σS^2 on the electron occupation number and the size of the QDs. Maximum power factor with value of 60 μW/cm K^2 for $n_{tot}=2$ is obtained when D is 3.6 and 4.4 nm. However, the maximum power factor for $n_{tot}=1.8$ can be found only when $D<3$ nm and the maximum power factor for $n_{tot}=2.2$ can be found only when $D>5$ nm. This feature indicates that the peak of power factor shifts to larger D when n_{tot} becomes larger.

Figure 6 shows the dependence of TE transport properties on n_{tot} for $D=3.6$, 3.8, and 4 nm. The decrease in n_{tot} can lead to an increase in the amplitude of Ξ as shown in Fig. 4(d) and a decrease in μ as shown in Fig. 3(b). The combination of these features make the dependence of the electrical conductivity σ on n_{tot} a little complicated. For $D=3.6$ and 3.8 nm case, σ decreases when n_{tot} increases. For $D=4$ nm case, σ increases when n_{tot} increases. The Seebeck coefficient S always increases when n_{tot} increases. The absolute value $|S|$ becomes larger for $D=3.6$ nm and 3.8 nm and becomes smaller for $D=4$ nm when n_{tot} increases. A maximum of power factor as large as 78 μW/cm K^2 can be obtained when $n_{tot}=1.9$ and $D=3.6$ nm as shown in Fig. 6(b).

The TE figure of merit ZT can be written as $ZT=\sigma S^2 T/(\kappa_e+\kappa_l)$, where κ_l is the lattice thermal conductivity. Figure 7 shows the dependence of ZT on D for different n_{tot} and on n_{tot} for different D. As mentioned earlier, the electronic thermal conductivity is calculated as $\kappa_e=[L^{22}-(L^{12})^2/L^{11}]/T$ using Eqs. (13a)–(13c). The lattice thermal conductivity κ_l is chosen to be 0.5 W/m K which is estimated to be the typical value of CdS/CdSe nanocomposites due to the phonon-interface scattering effect, as studied earlier by coauthor Yang.[23–25] Figure 7 shows a ZT over 0.55 can be found when n_{tot} is a little smaller than 2 for $D=3.6$ nm and when n_{tot} is a little larger than 2 for $D=4.4$ nm. Such a ZT value is much better than the state-of-the-art low-temperature TE materials,[61] and shows great promises in exploring the Kondo effect in strongly correlated quantum dot nanocomposites for low-temperature high-efficiency TE materials development.

We also note that, although we try to include the nonideal effects such as the effects of other scattering mechanisms on TE transport properties using the δ value derived from experimental mobility data, the consideration for temperature dependence of TE transport properties is not complete. Moreover, the high ZT value is not optimized in terms of temperature dependence. The key of this work is only to pointing a directions for low-temperature high-efficiency TE materials using quantum effects.

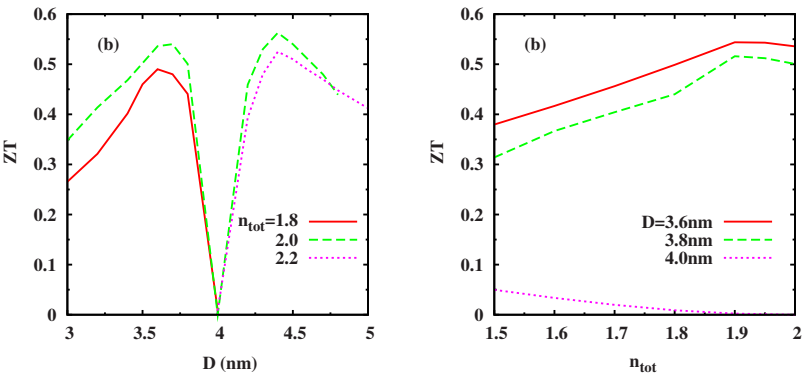

FIG. 7. (Color online) The dependence of ZT on (a) D for different $n_{tot}=1.8$, 1.9, and 2 (b) on n_{tot} for different $D=3.6$, 3.8, and 4 nm. The calculation uses inputs as $a=10$ nm, $\delta=3.6$ meV, $t=0.05$ eV, $T=77$ K, and $\kappa_l=0.5$ W/mK.

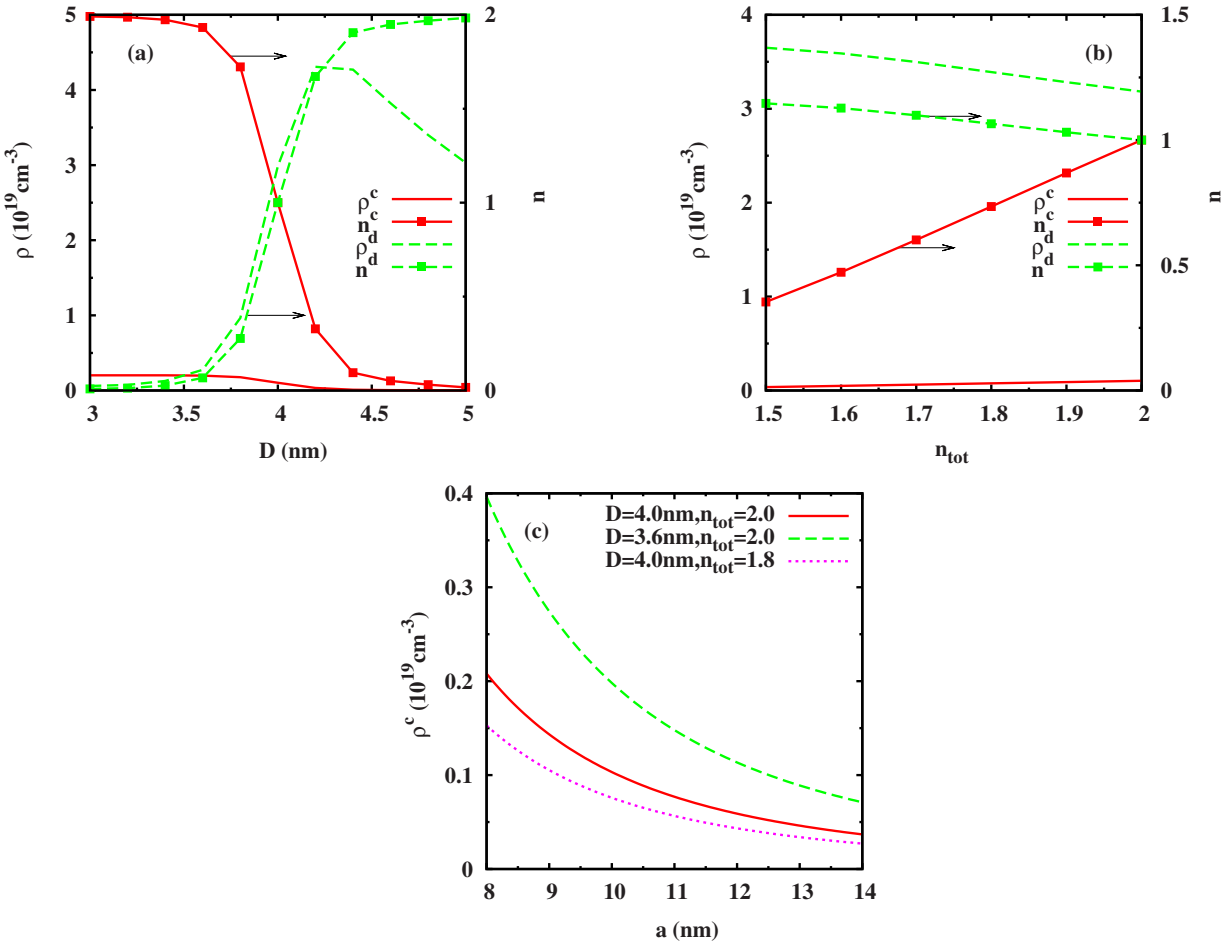

FIG. 8. (Color online) (a) Electron concentration ρ and occupation number n versus D when $n_{tot}=2$ and $a=10$ nm. (b) Electron concentration ρ and occupation number n versus n_{tot} when $D=4$ nm and $a=10$ nm. Solid curve: electron density in matrix. Dashed curve: electron density in QD. Solid curve with dot: occupation number in matrix. Dashed curve with dot: occupation number in QD. $T=77$ K. (c) Electron density as a function of a for fixed D and n_{tot}.

IV. CONCLUSION

The periodic Anderson model has been applied to study the TE transport properties in strongly correlated quantum dot nanocomposites at low temperature (77 K). The model is solved numerically using dynamical mean-field theory and the transport coefficients are calculated using the Kubo formula. We found that the energy bands with very sharp DOS can be formed in strongly correlated quantum dot nanocomposites. The asymmetry of the energy bands, the chemical potential, and the energy-sensitive Kondo scattering are highly dependent on the parameters such as the size of QD and the electron occupation number which can be controlled by the doping concentration in QDs and matrix, the size of QDs and the interdot spacing. For one certain set of parameters ($D=4$ nm and $n_{tot}=2$ in our calculation) when $\varepsilon_d-\varepsilon_c=-U/2$ and $n_{tot}=2$ is satisfied, i.e., the particle-hole symmetry is achieved, the Seebeck coefficient is exactly zero. Transition between n-type like behavior (with negative Seebeck coefficient) and the p-type like behavior (with positive Seebeck coefficient) is found when D and n_{tot} changes. Large Seebeck coefficient about 260 μV/K is obtained along with moderate electrical conductivity in the order of $10^5/\Omega$ m. A maximum of power factor about 78 μW cm K^2 can be found when $D=3.6$ nm, $n_{tot}=1.9$, and $\delta=3.6$ meV, where δ is calculated from the experimental mobility value. A not-optimized large ZT over 0.55 at 77K indicates great promises for using strongly correlated quantum dot nanocomposites as high-efficiency TE materials at low temperature.

ACKNOWLEDGMENTS

This work is supported by AFOSR (DCT Grant No. FA9550-08-1-0078 and MURI Grant No. FA9550-06-1-0326) and NSF (CMMI Grant No. 0729520 and CBET Grant No. 0846561). The authors also would like to acknowledge the valuable comments from the anonymous referee.

APPENDIX: ELECTRON FILLING

The electron doping concentration in the QDs and the matrix material can be written as $\rho^d=n^d/(\pi D^3/6)$ and $\rho^c=n^c/(a^3-\pi D^3/6)$, respectively. These relations indicate that n^d can be controlled by ρ^d and D, n^c can be controlled by ρ^c, D, and a. Usually, the studies of periodic Anderson model problems presents material properties directly through n_{tot}

rather than doping concentration. We thus presented the transport properties in strongly correlated quantum dot nanocomposites system with various n_{tot} rather than doping concentration in this paper. In order to give an intuitive sense on how electron distributes in the strongly correlated quantum dot nanocomposites system when a n_{tot} value is presented, we plot in Fig. 8 the electron densities and the electron occupation numbers in both QDs (ρ^d and n^d) and matrix (ρ^c and n^c) as functions of D, n_{tot}, and a. One can see that ρ^c is in the order of 10^{18} cm^{-3} and ρ^d is from nearly zero to 4×10^{19} cm^{-3}. Both ρ^c, n^c decrease and ρ^d, n^d increase when D increases because ε_d shifts to lower energy that leads to more electrons distributing in QDs and less electrons distributing in matrix when D increases. At the same time, the chemical potential μ shifts to lower energy as shown in Fig. 3(a) when n^c reduces. Similar trends are observed for $n_{tot} = 1.8$ and 2.2. Moreover, ρ^c, n^c increase and ρ^d, n^d decrease with n_{tot} increases. The reason is that μ always increases with n_{tot} increases as shown in Fig. 3(b) that leads to more electrons distributing in matrix. The dependence of ρ^c on a is simple as shown in Fig. 8(c). ρ^c decreases with a increases for fixed n_{tot} and D. The presentation in Fig. 8 tells a possibility to control n_{tot} and μ through doping concentration and size tuning in quantum dot nanocomposites.

*ronggui.yang@colorado.edu

[1] G. D. Mahan, Solid State Phys. **51**, 81 (1997).
[2] C. Grenzebach, F. B. Anders, G. Czycholl, and T. Pruschke, Phys. Rev. B **74**, 195119 (2006).
[3] A. T. Burkov and M. V. Vedernikov, in *CRC Handbook of Thermoelectrics*, edited by D. M. Rowe (CRC Press, Boca Raton, 1995).
[4] S. Paschen, in *Thermoelectrics Handbook: Macro to Nano*, edited by D. M. Rowe (CRC Press, Boca Raton, 2006).
[5] J. Hubbard, Proc. R. Soc. London, Ser. A **281**, 401 (1964).
[6] J. Kondo, Prog. Theor. Phys. **32**, 37 (1964).
[7] N. E. Bickers, D. L. Cox, and J. W. Wilkins, Phys. Rev. Lett. **54**, 230 (1985).
[8] I. Terasaki, I. Tsukada, and Y. Iguchi, Phys. Rev. B **65**, 195106 (2002).
[9] P. W. Anderson, Phys. Rev. **124**, 41 (1961).
[10] T. Saso and K. Urasaki, J. Phys. Soc. Jpn. **71**, suppl. 288 (2002).
[11] H. Schweitzer and G. Czycholl, Phys. Rev. Lett. **67**, 3724 (1991).
[12] D. Goldhaber-Gordon, H. Shtrikman, D. Mahalu, D. Abusch-Magder, U. Meirav, and M. A. Kastner, Nature (London) **391**, 156 (1998).
[13] S. M. Cronenwett, T. H. Oosterkamp, and L. P. Kouwenhoven, Science **281**, 540 (1998).
[14] H. Jeong, A. M. Chang, and M. R. Melloch, Science **293**, 2221 (2001).
[15] S. Sasaki, S. De Franceschi, J. M. Elzerman, W. G. van der Wiel, M. Eto, S. Tarucha, and L. P. Kouwenhoven, Nature (London) **405**, 764 (2000).
[16] W. G. van der Wiel, S. De Franceschi, T. Fujisawa, J. M. Elzerman, S. Tarucha, and L. P. Kouwenhoven, Science **289**, 2105 (2000).
[17] T. A. Costi and V. Zlatić, Phys. Rev. B **81**, 235127 (2010).
[18] A. I. Boukai, Y. Bunimovich, J. Tahir-Kheli, J. K. Yu, W. A. Goddard III, and J. R. Heath, Nature (London) **451**, 168 (2008).
[19] A. I. Hochbaum, R. K. Chen, R. D. Delgado, W. J. Liang, E. C. Garnett, M. Najarian, A. Majumdar, and P. D. Yang, Nature (London) **451**, 163 (2008).
[20] R. Venkatasubramanian, E. Siivola, T. Colpitts, and B. O'Quinn, Nature (London) **413**, 597 (2001).
[21] T. C. Harman, P. J. Taylor, M. P. Walsh, and B. E. LaForge, Science **297**, 2229 (2002).
[22] T. C. Harman, P. J. Taylor, D. L. Spears, and M. P. Walsh, J. Electron. Mater. **29**, L1 (2000).
[23] R. G. Yang and G. Chen, Phys. Rev. B **69**, 195316 (2004).
[24] R. G. Yang, G. Chen, and M. S. Dresselhaus, Phys. Rev. B **72**, 125418 (2005).
[25] M. S. Jeng, R. G. Yang, D. Song, and G. Chen, J. Heat Transfer **130**, 042410 (2008).
[26] J. Martin, L. Wang, L. D. Chen, and G. S. Nolas, Phys. Rev. B **79**, 115311 (2009).
[27] A. Popescu, L. M. Woods, J. Martin, and G. S. Nolas, Phys. Rev. B **79**, 205302 (2009).
[28] A. J. Minnich, H. Lee, X. W. Wang, G. Joshi, M. S. Dresselhaus, Z. F. Ren, G. Chen, and D. Vashaee, Phys. Rev. B **80**, 155327 (2009).
[29] S. V. Faleev and F. Léonard, Phys. Rev. B **77**, 214304 (2008).
[30] M. Zebarjadi, K. Esfarjani, A. Shakouri, J. H. Bahk, Z. X. Bian, G. H. Zeng, J. Bowers, H. Lu, J. Zide, and A. Gossard, Appl. Phys. Lett. **94**, 202105 (2009).
[31] M. Zebarjadi, K. Esfarjani, A. Shakouri, J. H. Bahk, Z. X. Bian, G. H. Zeng, J. Bowers, H. Lu, J. Zide, and A. Gossard, J. Electron. Mater. **38**, 954 (2009).
[32] M. S. Dresselhaus, G. Chen, M. Y. Tang, R. G. Yang, H. Lee, D. Z. Wang, Z. F. Ren, J. P. Fleurial, and P. Gogna, Adv. Mater. **19**, 1043 (2007).
[33] D. L. Medlin and G. J. Snyder, Curr. Opin. Colloid Interface Sci. **14**, 226 (2009).
[34] B. Poudel, Q. Hao, Y. Ma, Y. C. Lan, A. Minnich, B. Yu, X. Yan, D. Z. Wang, A. Muto, D. Vashaee, X. Y. Chen, J. M. Liu, M. S. Dresselhaus, G. Chen, and Z. F. Ren, Science **320**, 634 (2008).
[35] J. Zhou, X. B. Li, G. Chen, and R. G. Yang, Phys. Rev. B (to be published).
[36] G. D. Mahan and J. O. Sofo, Proc. Natl. Acad. Sci. U.S.A. **93**, 7436 (1996).
[37] A. A. Balandin and O. Lazarenkova, Appl. Phys. Lett. **82**, 415 (2003).
[38] A. Yadav, K. P. Pipe, W. Ye, and R. S. Goldman, J. Appl. Phys. **105**, 093711 (2009).
[39] I. Gómez, F. D. Adame, E. Diez, and P. Orellana, J. Appl. Phys. **92**, 4486 (2002).
[40] R. Y. Wang, J. P. Feser, J. S. Lee, D. V. Talapin, R. Segalman, and A. Majumdar, Nano Lett. **8**, 2283 (2008).
[41] Th. Pruschke, D. L. Cox, and M. Jarrell, Phys. Rev. B **47**, 3553 (1993).
[42] T. Kasuya, Prog. Theor. Phys. **16**, 45 (1956); M. A. Ruderman

and C. Kittle, Phys. Rev. **96**, 99 (1954); K. Yosida, *ibid.* **106**, 893 (1957).
[43] H. Z. Song, K. Akahane, S. Lan, H. Z. Xu, Y. Okada, and M. Kawabe, Phys. Rev. B **64**, 085303 (2001).
[44] J. W. Cai and G. D. Mahan, Phys. Rev. B **76**, 205116 (2007).
[45] J. W. Cai and G. D. Mahan, Phys. Rev. B **78**, 035115 (2008).
[46] F. X. Redl, K. S. Cho, C. B. Murray, and S. O'Brlen, Nature (London) **423**, 968 (2003).
[47] A. Georges, G. Kotliar, W. Krauth, and M. J. Rozenberg, Rev. Mod. Phys. **68**, 13 (1996).
[48] A. Stoyanova, C. Sousa, C. de Graaf, and R. Broer, Int. J. Quantum Chem. **106**, 2444 (2006).
[49] G. Kotliar, S. Y. Savrasov, K. Haule, V. S. Oudovenko, O. Parcollet, and C. A. Marianetti, Rev. Mod. Phys. **78**, 865 (2006).
[50] H. Schweitzer and G. Czycholl, Solid State Commun. **74**, 735 (1990).
[51] H. Schweitzer and G. Czycholl, Z. Phys. B: Condens. Matter **83**, 93 (1991).
[52] N. Grewe and F. Steglich, in *Handbook on the Physics of Rare Earths*, edited by K. A. Gschneidner, Jr. and L. Eyring (North-Holland, Amsterdam, 1991).
[53] W. Metzner and D. Vollhardt, Phys. Rev. Lett. **62**, 324 (1989).
[54] G. D. Mahan, *Many-Particle Physics*, 3rd ed. (Plenum, New York, 2000).
[55] G. Czycholl and H. J. Leder, Z. Phys. B: Condens. Matter **44**, 59 (1981).
[56] H. Schweitzer and G. Czycholl, Z. Phys. B: Condens. Matter **79**, 377 (1990).
[57] T. A. Costi, A. C. Hewson, and V. Zlatic, J. Phys.: Condens. Matter **6**, 2519 (1994).
[58] *Semiconductors. Physics of II-VI and I-VII Compounds*, Landolt-Börnstein, New Series, Group III, Vol. 17, Pt. b, edited by O. Madelung (Springer-Verlag, Berlin, 1982).
[59] A. I. Ekimov and A. A. Onuzchenko, Sov. Phys. Semicond. **16**, 1215 (1982); L. E. Brus, J. Chem. Phys. **80**, 4403 (1984); S. Rosen, O. Schwartz, and D. Oron, Phys. Rev. Lett. **104**, 157404 (2010); V. A. Fonoberov, E. P. Pokatilov, V. M. Fomin, and J. T. Devreese, *ibid.* **92**, 127402 (2004).
[60] K. Hess and H. Vana, J. Phys. C **6**, L150 (1973).
[61] J. R. Sootsman, D. Y. Chung, and M. G. Kanatzidis, Angew. Chem., Int. Ed. **48**, 8616 (2009).